

Final Draft
of the original manuscript:

Hoelzel, M.; Gan, W.M.; Hofmann, M.; Randau, C.; Seidl, G.; Juettner, P.;
Schmahl, W.W.:

**Rotatable multifunctional load frames for neutron diffractometers
at FRM II—design, specifications and applications**

In: Nuclear Instruments and Methods in Physics Research A (2013) Elsevier

DOI: 10.1016/j.nima.2013.01.049

Rotatable multifunctional load frame for neutron diffractometers at FRM II – design, specifications and applications

M. Hoelzel^a, W.M. Gan^b, M. Hofmann^a, C. Randau^c, G. Seidl^a, P. Jüttner^a, W. W. Schmahl^d

^a Technische Universität München, Forschungsneutronenquelle Heinz Maier-Leibnitz (FRM II), D-85747 Garching, Germany

^b German Engineering Materials Science Centre, Helmholtz-Zentrum Geesthacht, D-21502 Geesthacht, Germany

^c Georg-August Universität Göttingen, Geowissenschaftliches Zentrum, D-37077 Göttingen, Germany

^d Ludwig-Maximilians-Universität München, Department für Geo- und Umweltwissenschaften, D-80333 München, Germany

Corresponding author:

Dr. Markus Hoelzel

Email: markus.hoelzel@frm2.tum.de

Phone: +49 89 289 14314

Fax: +49 89 289 14911

Address : Lichtenbergstrasse 1, 85747 Garching near Munich, Germany

Abstract

Novel tensile rigs have been designed and manufactured at the research reactor Heinz Maier-Leibnitz (FRM II, Garching near Munich). Besides tensile stress and pressure, also torsion can be applied. The unique Eulerian cradle type design (ω , χ , and ϕ axis) allows orienting the sample with respect to the scattering vector. Applications of these tensile rigs at our neutron diffractometers enable various investigations regarding to structural changes under mechanical load, e.g. crystallographic texture evolution, stress-induced phase transformations or lattice expansion and the anisotropy of mechanical response.

Keywords: neutron diffractometer, load frame, tensile rig

1. Introduction

The understanding of structure property relationship is an essential condition for the development and improvement of engineering materials. Such investigations often involve *in-situ* characterization of materials under external load. In particular neutron diffraction offers the possibility to follow structural changes on a microscopic level in correlation with mechanical behaviour. In this respect neutron diffractometers are often equipped with load frames to investigate stress-induced phase transformations, lattice strain or crystallographic texture developments [1-5]. In general, neutron diffraction studies give complementary information to X-ray or synchrotron methods. Due to large penetration depths of neutrons even for wavelengths >1 Å, relatively large gauge volumes or bulk samples can be investigated, enabling even coarse-grained and gradient materials to be characterized easily.

At the research reactor FRM II the two neutron diffractometers SPODI and STRESS-SPEC are the instruments of choice for materials characterization [6]. The materials science diffractometer STRESS-SPEC is designed for strain and texture analysis. In addition, this instrument enables a fast collection of powder diffraction patterns, e.g. for the study of reaction kinetics, at a limited scattering angle range. The high-resolution powder diffractometer SPODI is designed for structure refinement on complex systems. Particular attention is paid to enable the characterization of functional materials under special environmental conditions. More details on the design, specifications and applications of the diffractometers SPODI and STRESS-SPEC can be found in the publications, respectively [7-9]. Both

48 instruments provide complementary capabilities for the structural investigations of materials under
49 mechanical load. For these applications two novel, compact load frames were designed for use on both
50 diffractometers.

51

52 The development of the load frames was driven by research projects carried out at the neutron
53 diffractometers at FRM II. Moreover, the load frames provide a broad range of applications for
54 materials investigations to the user community. Both frames allow to orient the load axis with respect
55 to the incident beam achieved by a χ -rotation axis. One rig (“uniaxial rig”) offers uniaxial tension and
56 compression which is optimized for texture analysis (e.g. pole figure measurements) by free sample
57 rotation around the φ -axis. The second rig (“multiaxial rig”) enables in addition to
58 tension/compression the application of torsion.

59

60 In this contribution, we report on the design and specifications of the new tensile rigs. First results of
61 experiments on nickel titanium shape memory alloys are also presented.

62

63 **2. Layout, specifications and data acquisition**

64

65 **2.1 Design and specifications**

66

67 The two load frames are illustrated in figure 1 showing the commonalities as well as their differences.
68 Both rigs are designed for a maximum load of 50 kN in tension or compression and share a common
69 basis structure. They are constructed as double column machines attached to identical rotation frames.
70 This allows to remotely rotate the load axis around 90° from a horizontal to a vertical setup. This
71 rotation is exactly the same as the χ -rotation as used in a standard Eulerian cradle. The χ -tilting of a
72 tensile rig is achieved by a stepper motor and monitored by an optical encoder. The base plate of the
73 rotation frame can be leveled out by a three point fixture as well as positioned in x- and y-directions by
74 adjustment screws.

75

76 Tensile axis (for tensile and compressive force) and torsion axis (in case of the multiaxial rig) are
77 equipped with servo motors and load cells or a torque sensor, respectively. The motors are attached to
78 the axis via cam belts. The uniaxial rig allows an additional rotation (φ - rotation) of the sample around
79 the load axis under full load using a stepper motor (figure 2). In case of the multiaxial rig the stepper
80 motor is substituted by a servo motor providing a torque of 100 Nm (figure 3). The load cell of the
81 multiaxial rig is constructional decoupled from the torsion axis so that no torque acts on it.

82

83 Both load frames come with a range of grips and additional equipment like furnaces (see chapter 2.3).
84 Their compact design makes them highly portable and enables usage also on other instruments. An
85 overview of the main design specifications are summarized in table 1.

86

87 **2.2 Control and data acquisition**

88

89 The load frames are controlled by electronics and software purchased from DOLI Company. Both axes
90 corresponding to tensile stress/compression and torsion can be operated in following modes: constant
91 load or cycling with fixed amplitude. The load increase can be carried out either stepwise or in a
92 continuous mode. In general, continuous loading enables fast data collection and diminishes creep or
93 stress relaxation effects [1]. The axes for stress/compression and torsion can be controlled
94 independently or synchronized. Experiments can be carried out either under load control, position
95 control or strain control mode.

96

97 A common interface to the data acquisition system (DAQ) of the diffractometers SPODI and STRESS-
98 SPEC was developed in house so that the tensile rigs can be operated under remote control. Following
99 target values can be set via DAQ: load, torsion, sample extension (i.e. “strain”) or alternatively position
100 of the crossbar (i.e. “position”) as well as the torsion angle. The speed to reach each value can also be
101 set independently.

102
103 The axes for χ - and ϕ -rotation are integrated as standard motors into the instrument control software.
104 Together with the rotation of the main sample table (ω -axis) the sample can be oriented with respect to
105 the incident beam by an Eulerian cradle like movement. The ϕ -axis supports pole figure measurements
106 either by a step scan (e.g. with a $5 \times 5^\circ$ grid) or a continuous scan (which can reduce the positioning time
107 considerably [8]). Furthermore the number of detected grains is increased up to a factor of 10 using the
108 continuous scan method, which improves grain statistics.

109 110 **2.3 Auxiliary Equipment**

111
112 Grips for tension and compression experiments were designed for standard samples referring to DIN
113 50125. The specimens shape can be round with maximum diameter of 10 mm or rectangular with a
114 maximum width of 6 mm depending on the material. For torsion experiments a modified sample
115 geometry based on round standard samples was developed to avoid slip of the sample under torque.
116 The macroscopic strain is usually measured by clip-on extensometers. Additionally a camera based
117 system is available for contact-free recording of the sample extension. In order to enable experiments
118 under mechanical load and high temperatures a mirror furnace for the tensile rigs was developed and
119 successfully applied in first experiments up to 1000 °C.

120 121 **3. Experimental examples**

122
123 Force and torque sensors of the load frames were calibrated by means of certified sensors. First test
124 experiments using different modes were performed on steel samples [10]. In the following we report on
125 neutron diffraction studies on nickel titanium shape memory alloys.

126 127 **3.1 *In-situ* structure analysis at SPODI**

128
129 Experiments at the high-resolution diffractometer SPODI were carried out to study the anisotropy of
130 the mechanical response of nickel titanium shape memory alloys with a nominal composition of 50.14
131 at.% Ni and monoclinic symmetry (space group $P2_1/m$). The multiaxial load frame was set to a fixed ω -
132 orientation of 45° with respect to the incident beam. Diffraction patterns were collected using a
133 wavelength of 2.536 Å at different strain levels up to 4% strain. The load frame was operated in strain
134 control mode to achieve a constant strain level during the data collection. At each strain level,
135 measurements in different χ -orientations were performed. The analysis of the data yielded the changes
136 in d-values and intensities for various Bragg reflections. These results were used to derive elastic
137 constants based on an approach by Popa [11]. The measurements allowed the separation of the
138 anisotropic elastic strain of the material from the anisotropic pseudoplastic strain of the monoclinic
139 martensite phase of NiTi. The pseudoplastic strain was attributed to the adaption of the ferroelastic twin
140 domain structure to the applied stress, which is the key mechanism for the shape memory effect. The
141 ferroelastic twinning/detwinning process was visible from changes in the intensity distribution of the
142 neutron diffraction maxima.

143
144

3.2 *In-situ* texture analysis of NiTi at STRESS-SPEC

In-situ texture analysis provides an option to come closer to materials processing (heating, tension, compression, torsion, etc.). Similar activities can also be carried out at synchrotron source. However, the maximum detected gauge volume ($\sim 1 \text{ mm}^3$) limits its application for the analysis on bulky properties of coarse grained materials. Moreover, the most loading machines are without χ -tilting and ϕ -rotation which produces two disadvantages. First, only incomplete pole figures were obtained, as reported in paper [13] the pole figure with centre of a 20° non-measured region. This will lead to a lower quality ODF calculation due to the less input data, especially for non-cubic structural materials. Second, under one setup it is impossible to simultaneously obtain intensity, peak position and FWHM pole figures without χ -tilting. One must tilt the sample normal to the beam direction to obtain axial strains. The first application of our load frame to investigate intensity, peak shift and peak broadening pole figures at one measurement was published in reference [10].

Specific example of tensile texture evolution on an identical NiTi is presented. To avoid the misorienting of the sample after each tensile strain *in-situ* is strongly required. And for ODF calculation on this monoclinic NiTi large numbers and high quality complete pole figures are also necessary. The measurement was carried out STRESS-SPEC with a wavelength of 1.67 \AA using the Si monochromator. The gauge volume was defined by a primary slit of $5 \times 5 \text{ mm}^2$ and radial collimator with a field of view of 5 mm . A position sensitive area detector of $300 \times 300 \text{ mm}^2$ covering a diffraction angle 2θ of about 15° at a sample to detector distance of 1040 mm was used to collect the diffracted neutron intensities.

According to previous structure analysis results from experiments carried out on the diffractometer SPODI, pole figures were measured at 0%, 4% and 8% strain, respectively. At each strain value the standard equal angular scan method for complete pole figure measurement was used. The scan involves data collection after a stepwise change of the χ -angle from 0° to 90° during a complete ϕ -angle rotation from 0° to 360° at each χ -position. A scanning routine was implemented [8] to collect all the diffraction patterns while the ϕ -axis is rotated continuously with a speed of 5° in 90 seconds. A complete pole figure at one detector position took a total measurement time of 10 hours. Three detector positions were needed to obtain 10 reflections of the monoclinic NiTi alloy in order to calculate the orientation distribution function (ODF). Figure 4 shows a 2D image and its summed diffraction pattern at the first detector position at $2\theta = 42.4^\circ$. The software package StressTextureCalculator (SteCa) [12] was used to extract the pole figures from the measured data.

Figure 5 shows the development of the pole figures with increasing strain of 0%, 4% and 8%, respectively. A radial concentration in the pole figures is observed from which the formation of a fibre texture can be deduced. The maximum intensity remains nearly stable till 8% strain. A gradual rotation of maximum poles / planes with increasing strain is obvious, which most likely arises from twinning deformation.

In addition, the high quality pole figures will enable us to calculate the complete Orientation Distribution Function (ODF) for the monoclinic martensite phase. This is in particular interesting as in monoclinic sample symmetry the calculation of the deformation components has seldom been performed till now and will contribute to our understanding of NiTi Shape Memory Alloys.

4. Summary

Novel tensile rigs were developed and set into operation at diffractometers STRESS-SPEC and SPODI at research reactor FRM II. The load frames allow tension, compression and torsion while the load can be applied in step wise fashion, cyclic mode or continuous mode. The unique Eulerian cradle type design enables to rotate the load axis with respect to the scattering geometry. Despite their high

194 performance, a compact design could be achieved, enabling the use of the tensile rigs on different
195 instruments. The capabilities of the load frames were demonstrated by neutron diffraction studies on
196 nickel titanium shape memory alloys.

197

198 **Acknowledgements**

199

200 The first tensile rig was funded by the German Ministry for Education and Research (BMBF) in frame
201 of project No 05KN7RD1 for instrumental developments at the diffractometer SPODI. We thank the
202 staff of mechanical workshop at Department of Physics of Technische Universität München, where the
203 load frames were manufactured. We gratefully acknowledge C. Merkel and C. Xia for their
204 contribution in experiments and data evaluation.

205

206 **References**

- 207 [1] K. An, D. Skorpenske, A. D. Stoica, D. Ma, X.-L. Wang, E. Cakmak, *Met and Mat Trans A.*, 42A
208 (2011) 95-99.
- 209 [2] K. An, W.B. Bailey, S.O. Craig, H. Choo, C.R. Hubbard, D.L. Erdman, *J. Neutron Research*, 15(3-
210 4) (2007), 207–213.
- 211 [3] A.M. Paradowska, A. Baczmański, S.Y Zhang, A. Rao, P.J. Bouchar, J. Kelleher, *Proc. 161st*
212 *Annual ISIJ Meeting (161 ISIJ)*, 25-27 Mar 2011, Tokyo, Japan.
- 213 [4] Y. Tsuchiya, H. Suzuki, T. Umeno, S. Machiya, K. Osamura, *Meas. Sci. Technol.* 21 (2010)
214 025904.
- 215 [5] T. R. Woodruff, V. B. Krishnan, B. Clausen, T. Sisneros, V. Livescu, D. W. Brown, M. A. M.
216 Bourke, R. Vaidyanathan, *Rev. Sci. Instr.* 81 (2010) 063903.
- 217 [6] J. Neuhaus, W. Petry, *Neutron News*, 18(2) (2007),13-15.
- 218 [7] M. Hofmann, G. A. Seidl, J. Rebelo-Kornmeier, U. Garbe, R. Schneider, R. C. Wimpory, U.
219 Wasmuth, U. Noster, *Mater. Sci. Forum.* 524-525 (2006) 211-216.
- 220 [8] H.-G. Brokmeier, W. M. Gan, C. Randau, M. Völler, J. Rebelo-Kornmeier, M. Hofmann, *Nucl.*
221 *Instr. A642* (2011) 87-92.
- 222 [9] M. Hoelzel, A. Senyshyn, N. Juenke, H. Boysen, W. Schmahl, H. Fuess., *Nucl. Instr. A 667* (2012)
223 32-37.
- 224 [10] W.M. Gan, C. Randau, M. Hofmann, H.-G. Brokmeier, M. Mueller, A. Schreyer, *J. Phys.. :*
225 *Conf. Ser.* 340 (2012) 012100.
- 226 [11] N. C. Popa, *J. Appl. Cryst.* 33 (2000), 103-107.
- 227 [12] C. Randau, U. Garbe, H.-G. Brokmeier, *J. Appl. Cryst.* 44 (2011) 641-646.
- 228 [13] H.-G. Brokmeier, Sang Bong Yi, N. J. Park, J. Homeyer, *Solid State Phenom.* 105 (2005) 55-60.
- 229

230 **Table 1: Specifications of both tensile rigs**

231

	tensile rig 1 “multiaxial”	tensile rig 2 “uniaxial”
max. force (for tensile stress / pressure)	50 kN	50 kN
max. cyclic loading frequencies	1 Hz	1 Hz
max. torque	100 Nm	-
max. torsion angle	+/- 49°	-
max. cyclic torsion frequencies	0.16 Hz	-
□-tilting axis	0 - 90°	0 - 90°
□ rotation axis	-	0 - 360°
max. travel of crossbar	50 mm	75 mm
width (space between columns)	200 mm	200 mm

232

233

234 Figure Captions

235

236 Figure 1: Engineering drawing of the tensile rigs. On the top: the common basis; down left: “multiaxial
237 version”; down right: “uniaxial version”

238

239 Figure 2: load frame 2 “uniaxial version” with control electronics

240

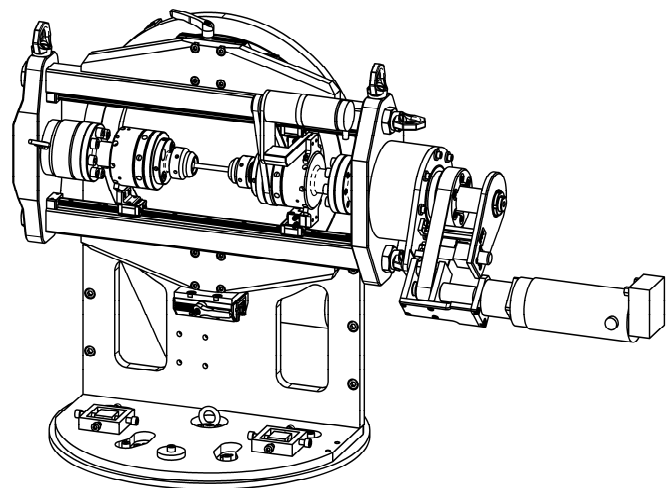
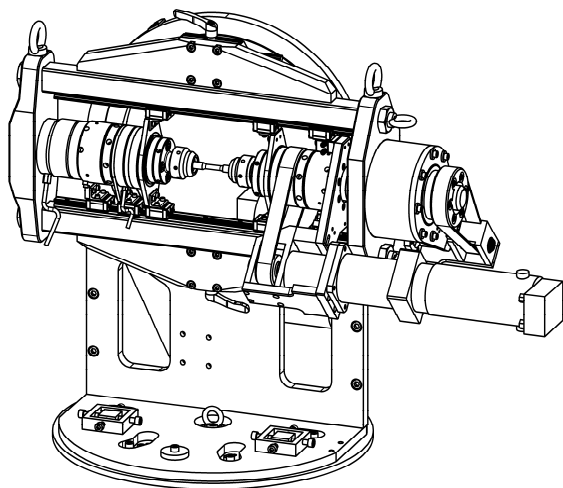
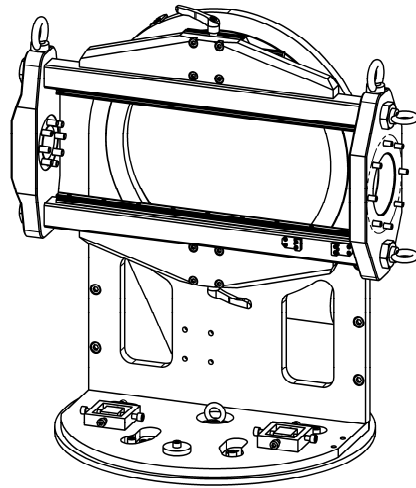
241 Figure 3: load frame 1 “multiaxial version” on high-resolution diffractometer SPODI

242

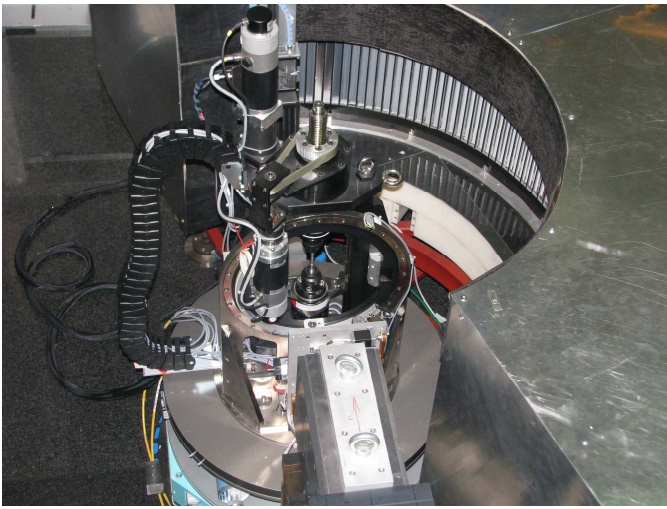
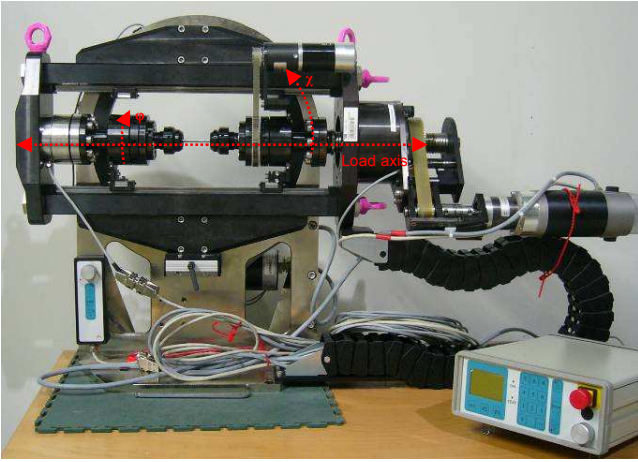
243 Figure 4: Detector image of NiTi (left) and its sum diffraction pattern (right) including (011), (100) and
244 (-110) reflections.

245

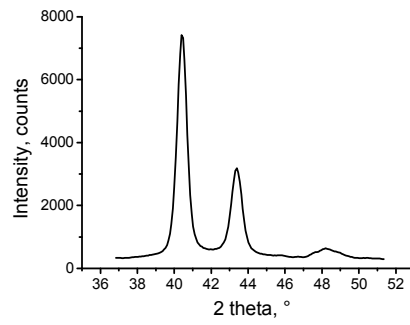
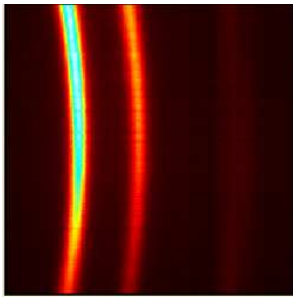
246 Figure 5: Evolution of (100) and (-110) pole figures from 0% to 8 % strain.

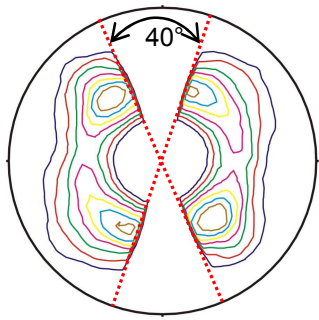


248
249
250
251
252
253
254
255
256
257
258
259
260
261



262
263
264
265
266
267
268
269
270
271
272
273
274
275





Incomplete (100) pole figure obtained using synchrotron

